Research article

MHD Maxwell dusty fluid in thermally stratified radiative flow with temperature-dependent thermal conductivity and Cattaneo-Christov model

Alugunuri Raghu [a,b], Nagaraju Gajjela [b,*], Mahesh Garvandha [c]

[a] Research Scholar, Department of Mathematics, School of CS&AI, SR University, Warangal, -506371, Telangana, India
[b] Department of Mathematics, School of CSE(AIML), SR University, Hanamkonda District, Telangana, PIN 506371, India
[c] Mathematics and Computing Skills Curriculum and Assessment Unit, Preparatory Studies Center, University of Technology and Applied Sciences-Shinas, Sultanate of Oman

ARTICLE INFO

ABSTRACT

It might be very important for the polymer processing industries to comprehend how Maxwell fluids behave on a stretched cylinder. Optimizing the extrusion and drawing processes can ensure the desired product qualities while avoiding faults. The objective of this study is heat transfer analysis on a Maxwell dusty fluid flow cylindrical surface with the Cattaneo-Christov concept. We immerse the cylinder in porous media, with a two-dimensional fluid regulating the flow. Our mathematical model further considers the effects of variable thermal conductivity, radiation, viscous and joule heating, magnetic field, thermal stratification, and slip velocity. Based on the presumptions, partial differential equations (PDE's) have been used to evolve the mathematical model. Using similarity transformations, the PDE's for heat and momentum for both phases are transformed into highly nonlinear ODE's. The numerical results have been obtained on these ordinary differential equations by using the RKF-45 method. This issue's main characteristic is that it examines the scenario's liquid and dust phases throughout. Results are given both visually and tabularly for the major parameters over a velocity, temperature, skin friction coefficient, and Nusselt number. When we compared our method to a previously published paper, we discovered a decent match. The findings, which were obtained for our system, show that the velocity and thermal gradient of both the phases of fluid and dust behave in an opposite trend in favor of rising Maxwell parameter, where the curvature parameter makes the rise in the same manner. Furthermore, the thermal transport profiles for both phases decline for the rising thermal time relaxation parameter.

1. Introduction

Heat transfer across stretched cylinders has use in several industrial settings, including heat exchangers in chemical operations, motor cooling systems, and thermal management in electronics. Its efficiency in engineering applications demonstrates its versatile character. Efficiency is critical for enhancing performance, ensuring safety, and optimizing energy consumption in many sectors. There are several industrial uses for MHD over stretched cylinders, including metallurgical operations where it improves fluid dynamics,

Nomenclature

B_0:	Constant magnetic field
a, b, c:	constants
B:	Slip parameter
$U_w(z)$:	stretching cylinder velocity
B_1	Velocity slip
Ec:	Eckert number
K:	Stoke's resistance constant $(6\pi r\mu)$
K_p:	Permeability parameter
K_∞ :	Free stream conductivity$(\mathrm{Wm^{-1}K^{-1}})$
$k^{'}$:	Permeability of the medium $(\mathrm{m^2})$
l	Characteristic length (m)
l^*:	Parameter of mass concentration
M:	Magnetic number
m:	Mass of dust particles
N:	Density number(dust particle)
Pr:	Prandtl number
Re_z:	Reynolds number
Rd:	Radiation parameter
T_0	Reference temperature
T_∞:	Ambient temperature
U_0	Reference velocity

Greek symbols

β:	Interaction parameter(velocity)
δ:	Thermal stratification parameter
β_1 :	Maxwell parameter
β_T:	Interaction parameter for temperature
ε:	small conductivity parameter
γ:	Curvature parameter
γ_1:	Specific heat parameter
λ:	thermal time relaxation
λ_1:	thermal time relaxation parameter
μ:	Dynamic viscosity
ρ, ρ_p	Fluid and particle phasedensity(with $\rho_p = mN$)
τ :	Relaxation time
τ_T:	Thermal equilibrium time
τ_v:	Time relaxation of particle phase

Abbreviations

MHD	Magnetic hydrodynamic
ODE's	Ordinary differential equations
RKF	Runge–Kutta-Fehlberg
PDE's	Partial differential equations
CC	Catteneo-Christov

aeronautical engineering where it optimizes aerodynamics, and nuclear reactors where it improves heat transfer. This innovative technique offers solutions for improved performance and efficiency in a range of sectors by controlling fluid flow using magnetic fields. Maxwell non-Newtonian visco-elastic fluids are a fascinating class of materials characterized by distinct rheological properties. These fluids are significant in a range of scientific and commercial applications because they combine properties of viscosity and elasticity and show complicated behavior under deformation. Understanding their unique characteristics is essential for optimizing workflows and developing innovative technical solutions. The Maxwell model is the simplest basic model for visco-elastic fluids and is effective for moderate dimensionless relaxation periods. Longer dimensionless relaxation times in highly concentrated polymeric fluids, however, may be accommodated by this approach. The specifics may be found in Fang-Hua Lin et al.'s literature [1]. The analytical solutions of the unsteady flow of an incompressible fractional Maxwell fluid between two infinite coaxial cylinders were studied by Jamil et al. [2] using integral transformations. They found that the shear stress corresponding to the Newtonian fluid is severe across the whole flow domain. Javed and Ghaffari [3] investigated numerically an incompressible Maxwell fluid in a steady two-dimensional flow across a stretched sheet at an oblique stagnation point. They found that when Deborah's number rises, so does the velocity. Many
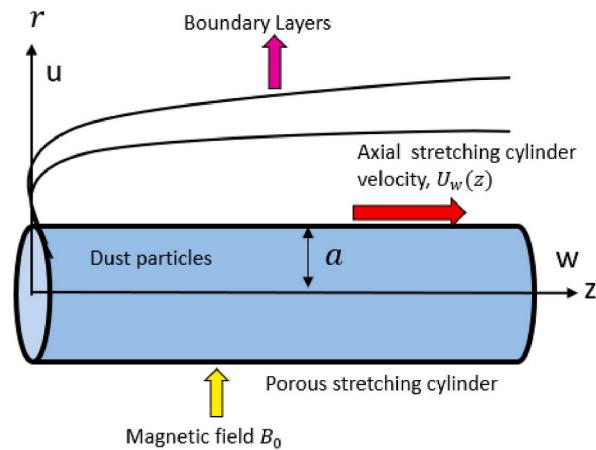
Fig. 1. Schematic diagram of flow of visco-elastic dusty fluid.

scholars have recently contributed to the study on Maxwell fluid flow across diverse geometries [[4–7]].

Heat conduction theory is altered by the Cattaneo-Christov (CC), an extension of Fourier's rule that incorporates finite thermal wave velocity. This modification fixes flaws in traditional models, particularly when there are rapid temperature fluctuations or microscale dimensions. Heat transfer properties may be more accurately anticipated by employing the CC formulation, which has applications in a variety of fields such as materials science, nanotechnology, and aeronautical engineering. The significance of this study lies in its potential to further our comprehension of thermal processes, hence facilitating the development of novel technologies and materials with enhanced thermal transport capabilities. Masood Khan et al. [8] conducted study on the 2D unsteady Maxwell fluid flow over the stretched cylinder using the CC Model. It was shown that lower values of the thermal relaxation parameter lead to less heat conduction. Saeed Islam et al. [9]looked into the mass and heat transfer mechanisms for a time-dependent Maxwell fluid flow in the presence of the CC theory. They observed that as the Maxwell and magnetic parameters rise, the velocity profile drops. Chunyan Liu et al. [10] investigated nonlinear radiative MHD Maxwell nano liquid flow via a stretched cylinder in a Darcy-Forchheimer porous medium. They observed that the velocity profile dropped as the Maxwell parameter value rose. Gayatri et al. [11] address the impact of heat source/sink interactions and variable thermal conductivity on nonlinear convective Maxwell fluid flow over a stretched sheet. It was revealed that the skin friction coefficient increases with an increase in the elastic parameter. Abiodun A. Opanuga et al. [12] looked into the unsteady MHD Maxwell fluid flow via an inclined stretched sheet with joule and viscous heating effects. They came to the conclusion that the temperature profile slows down with magnetic parameter. Sudarmozhi et al. [13] looked at the impacts of heat source/sink and the chemical interaction of Maxwell fluid over a porous stretched cylinder. They found that a visco-elastic fluid parameter is responsible for a diminishing velocity profile.

Different behaviors may be seen in dusty fluids, which are colloidal suspensions of particles in gases or liquids. Applications include material science, influencing aerosols, industrial processes, and environmental investigations. Thermal energy transport in dusty fluids is influenced by suspended particles in the fluid. Applications touch a variety of disciplines with distinct problems, ranging from industrial processes to atmospheric dynamics. The two-phase flow produced by a stretched cylinder immersed in a porous medium under radiation was examined in Manjunatha et al.'s work [14]. They observed that both the fluid and dust phases' velocities drop when the permeability parameter rises. The boundary layer flow of a dusty fluid suspended with Fe_2SO_4–Cu across a stretched sheet is examined by Radhika et al. [15], accounting for the effects of inhomogeneous heat source/sink, melting, and magnetic fields. They found that as the Hartmann number rises, the temperature and velocity gradients gradually diminish. Up to now, a lot of study has focused on the creation and use of two-phase fluids in a variety of settings, especially when it comes to cylinders [[16–18]].

Thermal stratification, a phenomenon where temperature layers form in a fluid, plays a crucial role in diverse natural and industrial processes. When coupled with variable thermal conductivity, it influences heat transfer mechanisms, impacting energy efficiency in engineering applications and ecological dynamics in natural systems. The effects of heat stratification on the movement of a dusty fluid over a porous stretched sheet were examined by researchers Gireesha et al. [19]. It was shown that the temperature and velocity profiles decrease as the thermal stratification parameter rises. The influence of thermal radiation and nanofluid on MHD Williamson fluid along a stretched cylinder in the presence of varying thermal conductivity was investigated by Bilal et al. [20]. Farooq et al. [21] analyzed MHD fluid flow with variable viscosity. Hayat et al. [22] found that temperature increases when variable thermal conductivity parameter rises in curved geometry. The radiation effect studied by Abbas et al. [23]with generalized slip condition. Recently Farooq et al. [24]considered magnetic field and Joule heating in inclined channel with slip effect. Using a variety of assumptions, many authors created concepts on the aforementioned impacts for the different flow models; refer to Refs. [[25–29]].

There hasn't been much attention from researchers to examine two-phase flow over cylindrical shape. Furthermore, there hasn't been a thorough discussion of the influence of thermal stratification and the CC model on extending cylinders in the literature. According to the literature study, no studies using dusty visco-elastic maxwell fluids have been reported. Motivated by previously cited data, the MHD of Dusty Maxwell fluid flow across a stretched cylinder has been performed. The literature study states that more investigation is required to ascertain the hydro magnetic impact on the permeable stretched flow of dust particles across a cylinder

subjected to variations in temperature, radiation, joule and viscous heating, velocity slip, and stratification effects. The required ordinary differential equations are numerically solved using the RKF iterative technique [[30,31]].

1.1. Mathematical formulation

Maxwell fluid in two dimensions is examined in a steady state with the addition of dust particles. The stretched surface of the porous material causes the incompressible flow. The cylinder's stretching velocity along its axis is $U_w(z)$, and the fluid flow direction is normal to the uniform magnetic field B = (0, B_0, 0). Assuming a low magnetic Reynolds number, the induced magnetic field is zero. The flow is produced linearly as a result of the permeable stretching surface, with the (u, w) and (u_p, w_p) components of velocity in the (r, z) directions, respectively. T and T_p, respectively, are used to represent the fluid and dust particle temperatures in Fig. 1. The Modified heat flux theory describes the phenomenon of thermal energy transmission in the flow. The formula for variable thermal conductivity is $K(T) = K_\infty(1 + \varepsilon\theta)$. Furthermore, Joule heating, viscous heating, and thermal radiation are all taken into account. The Maxwell fluid model [[6,11–13]] describes the viscoelastic type fluid's rheology as follows:

$$\frac{\partial w}{\partial z} + \frac{1}{r}\frac{\partial}{\partial r}(ru) = 0,\tag{1}$$

$$\left(u\frac{\partial w}{\partial r} + w\frac{\partial w}{\partial z}\right) + \tau\left(w^2\frac{\partial^2 w}{\partial z^2} + u^2\frac{\partial^2 w}{\partial r^2} + 2uw\frac{\partial^2 w}{\partial r\partial z}\right) = \frac{\mu}{\rho}\frac{1}{r}\frac{\partial}{\partial r}\left(r\frac{\partial w}{\partial r}\right) + \frac{KN}{\rho}(w_p - w) - \frac{\sigma B_0^2 w}{\rho} - \frac{\mu}{\rho k}w,\tag{2}$$

$$u_p\frac{\partial u_p}{\partial r} + w_p\frac{\partial w_p}{\partial z} = \frac{K}{m}(w - w_p),\tag{3}$$

$$\frac{\partial u_p}{\partial r} + \frac{u_p}{r} + \frac{\partial w_p}{\partial z} = 0,\tag{4}$$

$$\lambda\left(w^2\frac{\partial^2 T}{\partial z^2} + u^2\frac{\partial^2 T}{\partial r^2} + 2uw\frac{\partial^2 T}{\partial r\partial z} + w\frac{\partial w}{\partial z}\frac{\partial T}{\partial z} + u\frac{\partial w}{\partial r}\frac{\partial T}{\partial z} + w\frac{\partial u}{\partial z}\frac{\partial T}{\partial r} + u\frac{\partial u}{\partial r}\frac{\partial T}{\partial r}\right) + \rho C_p\left(u\frac{\partial T}{\partial r} + w\frac{\partial T}{\partial z}\right) = \frac{1}{r}\frac{\partial}{\partial r}\left(k(T)r\frac{\partial T}{\partial r}\right)$$
$$- \frac{1}{r}\frac{\partial}{\partial r}(rq_r) + \frac{\rho_p c_m}{\tau_T}(T_p - T) + \mu\left(\frac{\partial w}{\partial r}\right)^2 + \frac{\rho_p}{\tau_v}(w_p - w) + \sigma B_0^2 w^2,\tag{5}$$

$$\rho_p c_m\left(u_p\frac{\partial T_p}{\partial r} + w_p\frac{\partial T_p}{\partial z}\right) = -\frac{\rho_p c_m}{\tau_T}(T_p - T).\tag{6}$$

The following are the boundary conditions that apply to the aforementioned issue:

$$w = U_w(z) + B_1 v\frac{\partial w}{\partial r}, u = 0, T_w = T_0 + \frac{bz}{l}, at\ r = a,\tag{7}$$

$$w \to 0, w_p \to 0, u_p \to u, T_\infty = T_0 + \frac{cz}{l}, T_p \to T_\infty\ as\ r\to\infty,\tag{8}$$

where $U_w(z) = \frac{U_0 z}{l}$.

The corresponding variables listed below are recommended as

$$w = \frac{U_0 z}{l}f', u = \frac{-a}{r}\left(\frac{U_0 v}{l}\right)^{\frac{1}{2}}f(\eta), \eta = \frac{r^2 - a^2}{2a}\left(\frac{U_0}{vl}\right)^{\frac{1}{2}}, \theta(\eta) = \frac{T - T_\infty}{T_w - T_0}, \theta_p(\eta) = \frac{T_p - T_\infty}{T_w - T_0}, w_p = \frac{U_0 z}{l}F', u_p = -\frac{a}{r}\left(\frac{U_0 v}{l}\right)^{\frac{1}{2}}F(\eta).\tag{9}$$

Equation (9) may be substituted into equations (2)–(6) to obtain:

$$(1 + 2\eta\gamma)f''' + 2\gamma f'' + ff'' - (f')^2$$
$$+\beta_1\left(2ff'f'' - \frac{\gamma}{(1 + 2\eta\gamma)}f^2 f'' - f^2 f'''\right) + l^*\beta(F' - f') - (M + K_p)f' = 0,\tag{10}$$

$$-(F')^2 + FF'' + \beta(f' - F') = 0,\tag{11}$$

$$\frac{1}{Pr}\left[(1 + 2\eta\gamma)\{(1 + Rd + \epsilon\theta)\theta'' + Ec(f'')^2 + (\theta')^2\} + 2\gamma(1 + Rd + \epsilon\theta)\theta'\right] - \lambda_1\left[f^2\theta'' - ff'\theta' + (\delta + \theta)(f'^2 - ff'')\right] + f\theta'$$
$$- (\delta + \theta)f' + l^*\gamma_1\,\beta_T(\theta_p - \theta) + Ec\left(l^*\beta(F' - f')^2 + M(f')^2\right) = 0,\tag{12}$$

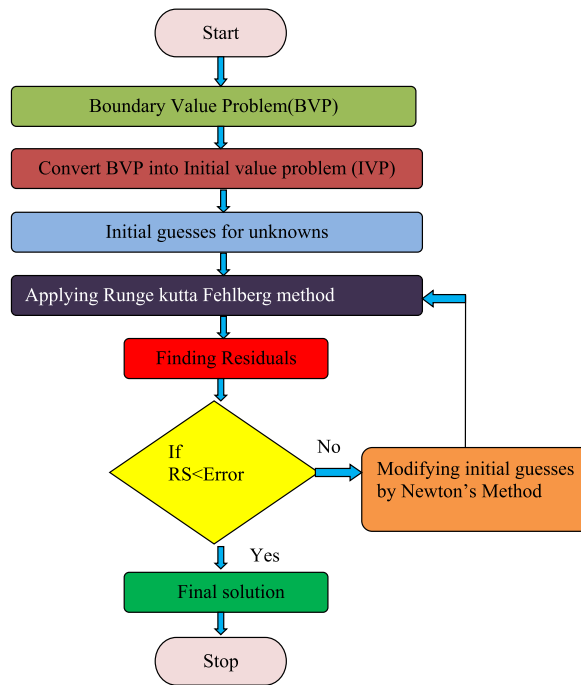$$-F\theta_p' + F'(\delta + \theta_p) + \beta_T(\theta_p - \theta) = 0.\tag{13}$$

Fig. 2. An explanation of the flow chart's numerical system.

The associated boundary conditions (7)–(8) are established as

$$f = 0, \ f' = 1 + Bf'', \theta = 1 - \delta \text{ at } \eta = 0, \tag{14}$$

$$f' = F = F - f = \theta = \theta_p = 0 \text{ as } \eta \rightarrow \infty. \tag{15}$$

1.2. Non-dimensional parameters

The following non-dimensional parameters, which are specified in the nomenclature table, were acquired in the present study.

$$\gamma = \left(\frac{\upsilon l}{a^2 U_0}\right)^{\frac{1}{2}}, M = \frac{\sigma l B_0^2}{\rho U_0}, l^* = \frac{\rho_p}{\rho} \text{ with } \rho_p = mN, \beta = \frac{l}{\tau_\upsilon U_0} \text{ with } \tau_\upsilon = \frac{m}{K}, \beta_1 = \frac{\tau U_0}{l}, K_p = \frac{l\upsilon}{U_0 k'}, B = B_1 \left(\frac{U_0 \upsilon}{l}\right)^{\frac{1}{2}}, \delta = \frac{c}{b}, Pr = \frac{\mu c_p}{k_\infty}, \beta_T = \frac{l}{U_0 \tau_T},$$

$$Ec = \frac{U_w^2}{c_p(T_w - T_\infty)}, Rd = \frac{16\sigma^* T_\infty^3}{3K_\infty k^*}, \gamma_1 = \frac{C_m}{C_p}, \lambda_1 = \frac{\lambda U_0}{l}.$$

1.3. Engineering quantities

In this research, the physical quantities of interest are the local Nusselt number and the skin friction, which are determined by

$$C_f = \frac{2\tau_w}{\rho U_w^2}, Nu_z = \frac{zq_w}{k(T_w - T_0)}, \tag{16}$$

where $\tau_w = \mu \left(\frac{\partial w}{\partial r}\right)_{r=a}$ and $q_w = -k\left(\frac{\partial T}{\partial r}\right)_{r=a} + (q_r)_{r=a}$.

The following are the physical quantities' non-dimensional forms:

$$C_f Re_z^{0.5} = 2f''(0), \tag{17}$$

$$Nu_z Re_z^{-0.5} = -(1 + Rd)\theta'(0), \tag{18}$$

where $Re_z = \frac{U_0 z^2}{\upsilon l}$.

Table 1
Comparison of $-f''(0)$.

γ	M	K_p	$-f''(0)$ Butt et al. [32]	$-f''(0)$ Present
0.25	0	1	1.5231	1.5239
0.5	0	1	1.6264	1.6291
1	0	0.5	1.6121	1.6342

Table 2
Comparison of $-\theta'(0)$ for $M = 0$.

γ	Pr	$-\theta'(0)$ Butt et al. [32]	$-\theta'(0)$ Present
0	1	1.0000	1.0159
	10	3.7207	3.6923

Table 3
Numerical values of $-C_f\sqrt{Re_z}$ and $Nu_z/\sqrt{Re_z}$ for $\beta = 0.4,\ l^* = 0.3, K_p = 0.5,\ Ec = 0.5,\ \lambda_1 = 0.2,\ \beta_T = 0.8,\ \gamma_1 = 0.5$.

γ	M	β_1	B	δ	Rd	Pr	ε	$-C_f\sqrt{Re_z}$	$Nu_z/\sqrt{Re_z}$
0.6	0.7	0.2	0.2	0.3	0.3	0.72	0.3	2.5400	0.6357
0.9								2.6701	0.7465
1.2								2.7937	0.8536
1.2	0.5	0.2	0.2	0.3	0.3	0.72	0.3	2.5940	0.8128
	1							2.7843	0.7574
	1.5							2.9471	0.7134
1.2	0.7	0.2	0.2	0.3	0.3	0.72	0.3	2.7563	1.1227
		1.2						2.8296	1.1041
		2.2						2.8968	1.0877
1.2	0.7	0.2	0.2	0.3	0.3	0.72	0.3	2.7563	0.8597
			0.4					2.1220	0.8719
			0.6					1.7327	0.8700
1.2	0.7	0.2	0.2	0.1	0.3	0.72	0.3	2.7563	1.0577
				0.3				2.7563	0.8597
				0.5				2.7563	0.6550
1.2	0.7	0.2	0.2	0.3	0.1	0.72	0.1	2.6740	0.7197
					0.6				0.9988
					1.2				1.3311
0.8	0.7	0.2	0.2	0.3	0.3	0.72	0.1	2.5891	0.7561
							0.3		0.7169
							0.5		0.6835
1	0.7	0.2	0.2	0.3	0.3	0.72	0.1	2.6740	0.8317
						1			0.8809
						1.5			0.9636

1.4. Method of numerical solution

The RKF-45 approach, which uses the MATLAB bvp4c process, is used for the nonlinear equation arrangement and boundary conditions (10)–(15). This method is solid at the fourth and fifth order, and the grid size of 0.01 is considered for 10^{-6} (Fig. 2).

2. Verification of findings

The findings of Tables 1 and 2 are verified by a comparison with the viscous fluid study of Adnan Saeed Butt et al. [32]; there is a significant and favorable connection between these investigations.

Table 3 shows that whereas greater values of *M, s, Re,* and *Kp* show the opposite trend, the amplitude of skin shear stress rises as the γ increases. The rate of heat transmission is likewise increased with increases in Pr and γ, whereas the rate of heat transfer is increased with Rd.

3. Results and discussion

Graphics are used to illustrate the effects of different relevant factors on axial velocity and temperature profiles in the fluid and dust phases and the findings are discussed theoretically. Solid lines indicate the fluid phase on all of the graphs, whereas dotted lines indicate the dust phase. Fig. 3 shows the influence of the curvature parameter (γ). As γ increases, the velocity profiles become better in
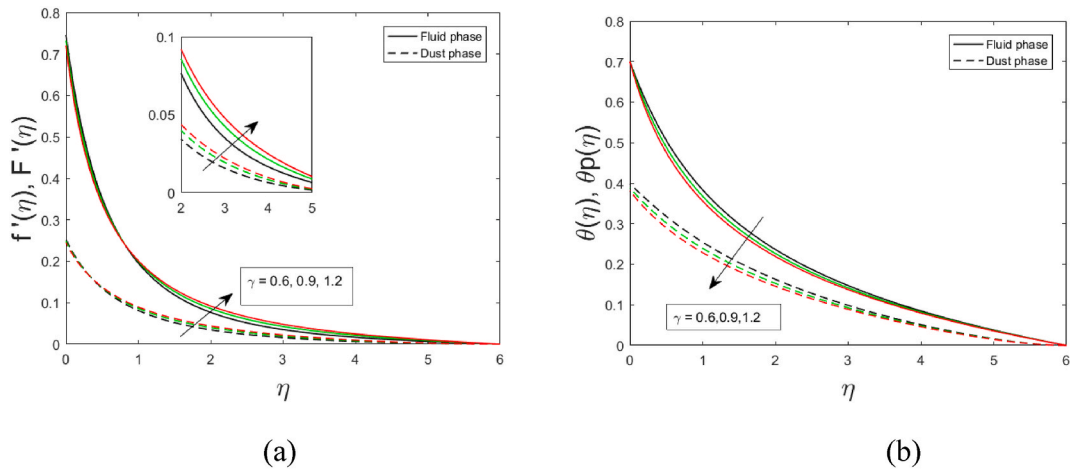
Fig. 3. The impact of γ on two parameters: (a) axial velocity and (b) temperature profile.
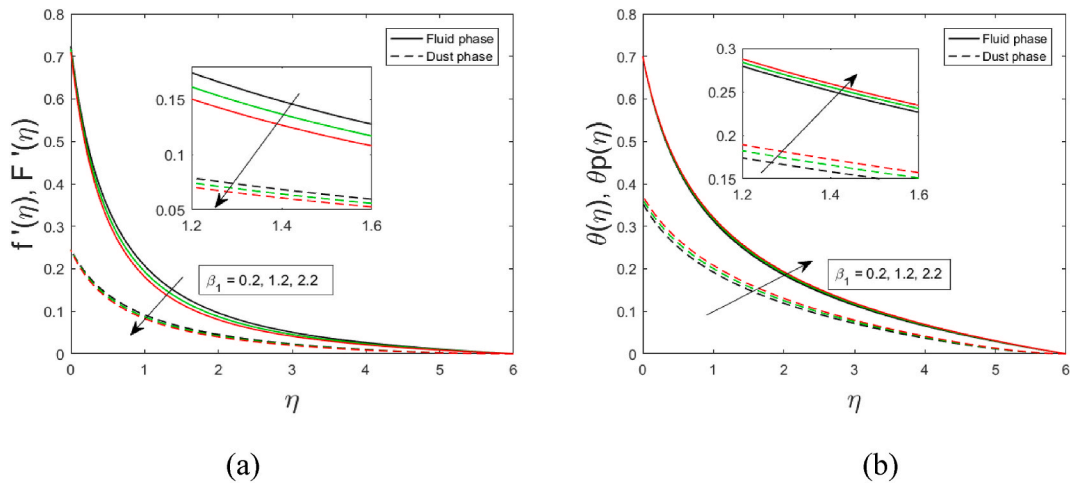

Fig. 4. The impact of β_1 on the following: a) axial velocity b) temperature profile.
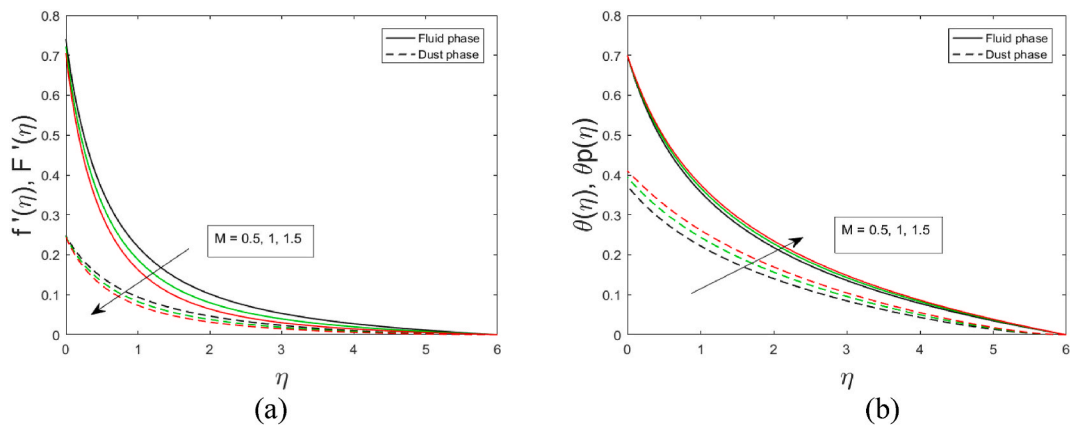

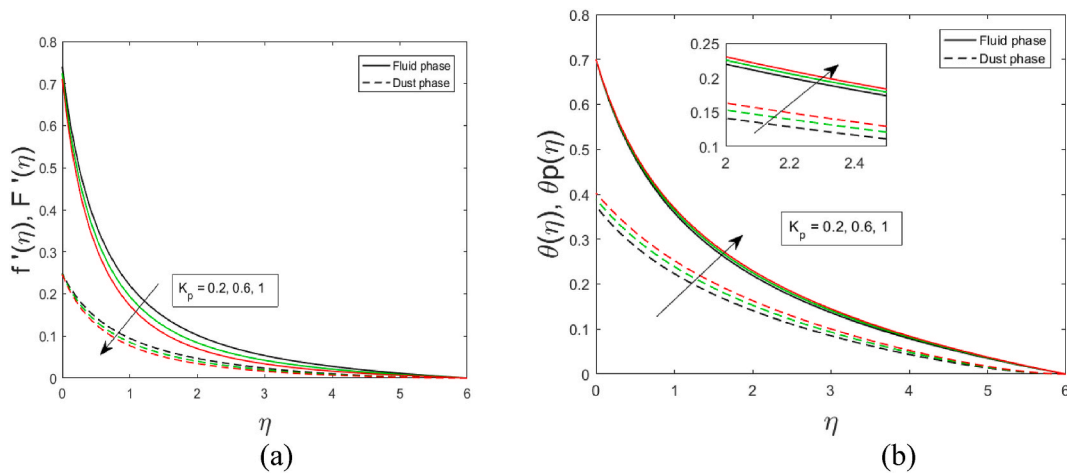**Fig. 5.** M's impact on the following: a) axial velocity b) temperature profile.

Fig. 6. K_p's impact on the following: a) axial velocity b) temperature profile.
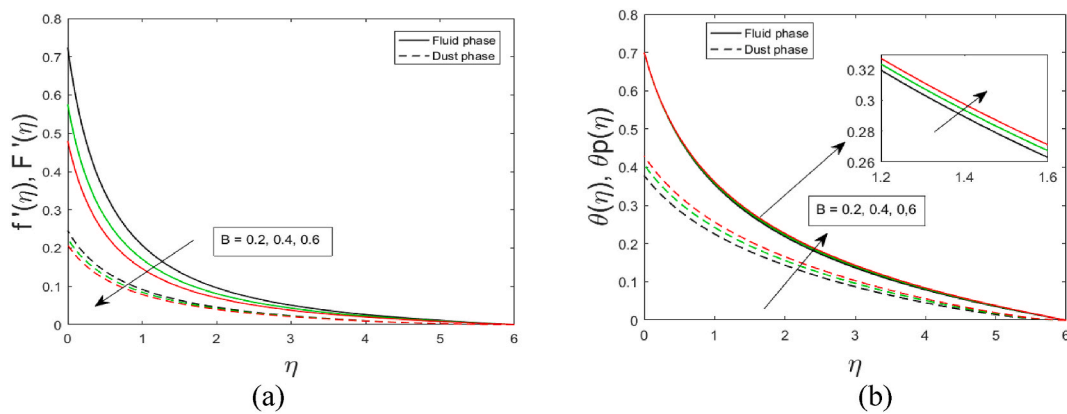

Fig. 7. Impact of B on a) axial velocity and b) temperature profile.

both phases. It is clear that when a cylinder is stretched as opposed to a flat surface, the boundary layer effects extend across a greater distance. The curvature of the Maxwell fluid around a stretched cylinder varies, affecting the fluid's axial velocity as well as its viscosity, stress distribution, and flow characteristics. However, with larger values of η, the opposite phenomenon is seen away from the cylinder. As can be seen in Fig. 2b–a bigger curvature actually causes a larger thermal boundary layer thickness, which lowers heat transfer rates because of the temperature increase at a certain distance from the cylinder.

The influence of the Maxwell fluid factor (β_1) on the temperature profiles and velocity was shown in Fig. 4. The stated velocity slows down as a result of higher β_1 (Maxwell fluid factor) values. Material reaction to deformation is represented by the Maxwell fluid parameter. This trend is brought about by the Maxwell parameter's tendency to reduce fluid viscosity as its values rise, lowering the yield stress. Higher values of the Maxwell parameter β_1 increase the flow's rate of heat transfer, as seen by the temperature field's graphical results. As previously shown, with higher values of β_1, the fluid behaves more like a solid, with fluid particles being near to one another. Consequently, there is an increase in thermal energy conduction within the fluid.

Fig. 5 shows the axial velocity fields and energy profiles for increasing magnetic parameter M values. The axial velocity of the system decreases as the magnetic field strength increases, and M gradually intensifies along the thermal profile. M (=0.5, 1, 1.5) is selected in order to carefully monitor the behavior of two curves. Similar variation can be seen in the thermal profiles for the dust and fluid phases. The magnetic parameter M increases the Lorentz force that occurs in the fluid flow due to applied magnetic field, and conflict force is created due to the rise in magnetic effect over a system that automatically reduces the velocity of the both phases.

The relevance of the permeability parameter impact in relation to the velocity and heat profiles is explained in Fig. 6. The velocity of the liquid decreases as the K_p is estimated higher. The existence of permeable material actually causes the liquid's flow to freeze, which causes the liquid's velocity to decline. As the values of K_p grow, the temperature gradient of both phases increases across the boundary.

Fig. 7 describes the influence of the wall slip parameter (B) on the velocity and temperature profiles. As the velocity slip parameter (B) raises, Fig. 6 shows that the velocity profile decreases and the temperature gradient profile increases. In practice, a cylinder's stretched impact is somewhat moved to the liquid layers, which causes f'(η) and F'(η) to drop while temperature rises as a consequence
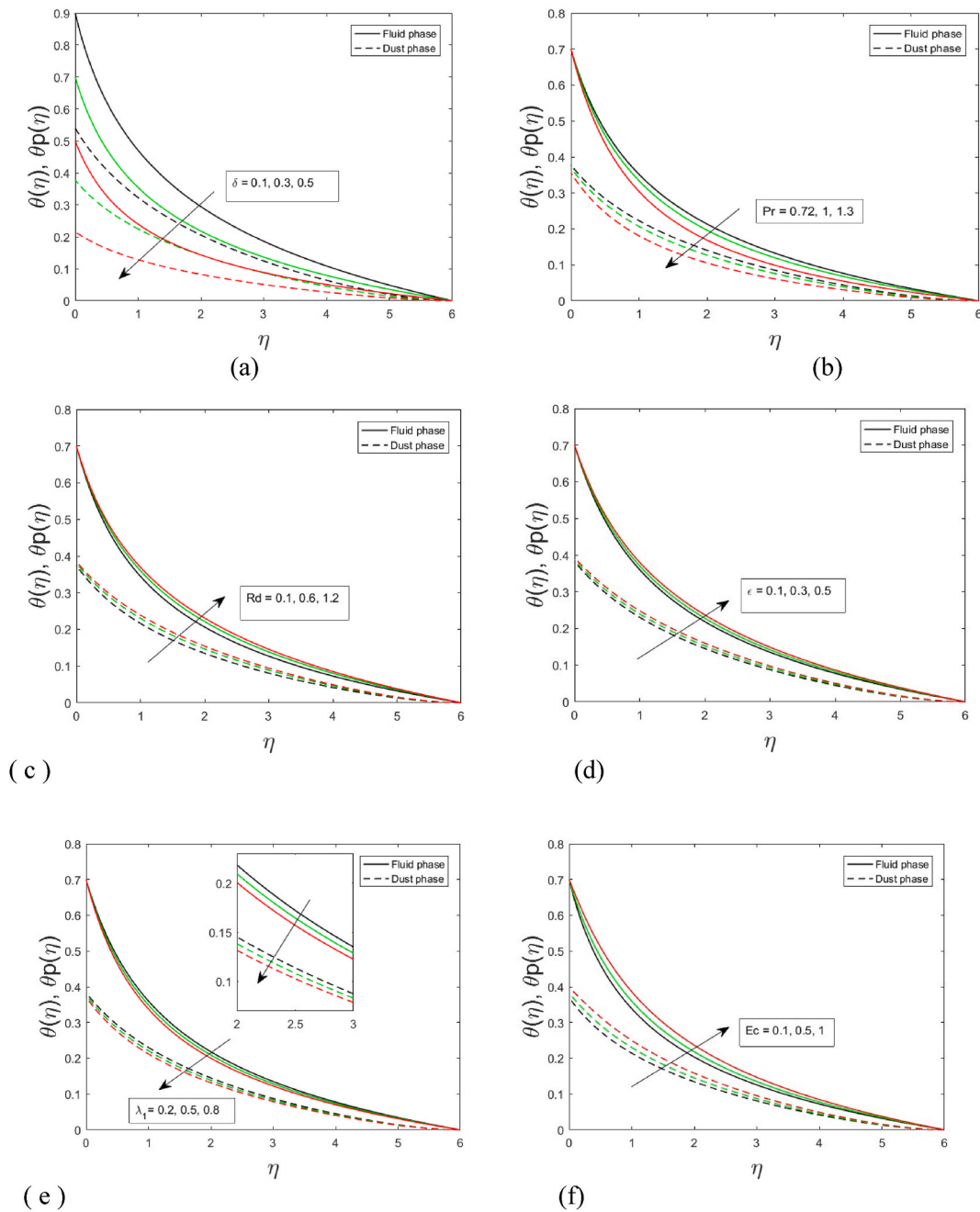
Fig. 8. Fluctuation in temperature for the following: a) Thermal Startification parameter (δ); b) Prandtl number (Pr); c) Radiation parameter (Rd); d) small conductivity parameter (ε); e) Thermal time relaxation parameter (λ_1); and f) Eckert number (Ec).

of increased interactions.

Plotted in Fig. 8a, the temperature profile is a decreasing function of the thermal stratification variable. In fact, with greater values of the stratification parameter, the temperature differential between the surface and the ambient temperature gradually reduces and drops significantly. As the Prandtl number (Pr) increases, the thickness of the thermal boundary layer decreases dramatically (see Fig. 8b). Since the momentum to thermal diffusivities ratio is known as the Prandtl number. Momentum diffusivity increases while thermal diffusivity decreases with increasing Pr. Temperature profile therefore decreases. Fig. 8c shows how the temperature gradient of the fluid and dust phases is affected by the radiation parameter (Rd). The radiation parameter Rd determines the proportionate contribution of conduction heat transfer to thermal radiation transport. It is evident that a rise in the radiation parameter results in an increase in the boundary layer's temperature. The thermal boundary layer thickness is enhanced, as predicted, by an increase in the thermal radiation parameter. As seen in Fig. 8d thermal boundary layer thickness is increased in both phases for small thermal
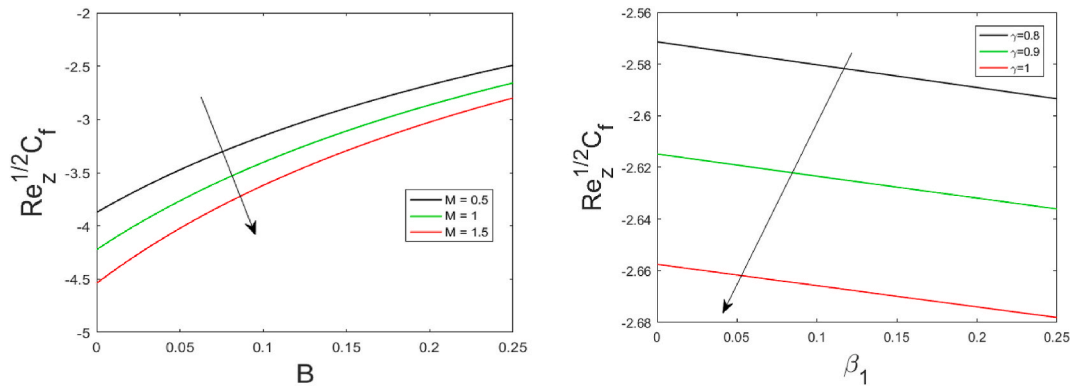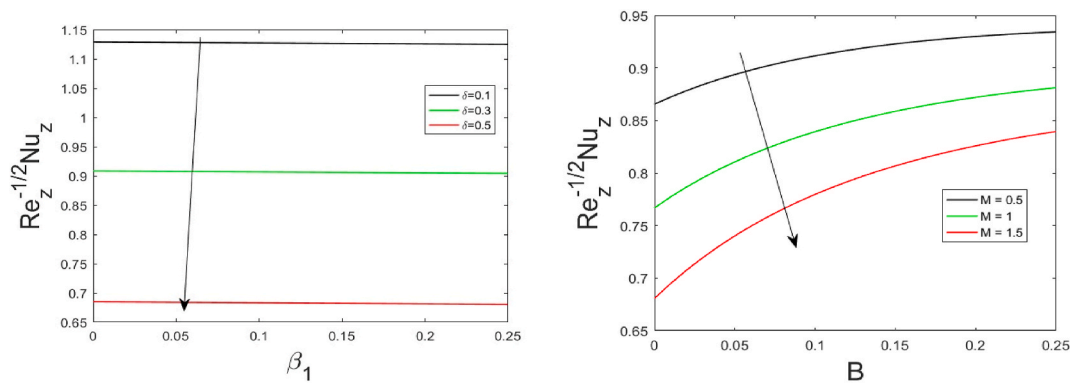
Fig. 9. M and γ's effect on $C_f Re_z^{0.5}$.

Fig. 10. δ and M's effect on $Re_z^{-0.5} Nu_z$.

conductivity parameters (ε). As the fluid's temperature improved, the liquid's thermal conductivity improved both physically and in terms of variable thermal conductivity. The influence of thermal relaxation time parameter λ_1 on the rate of heat transfer is seen in Fig. 8e. The two-phased temperature decreases as the thermal relaxation time parameter increases. Higher values of the relaxation time parameter in the CC heat flow model physically regulate how quickly heat waves spread across a particular material. Heat transfer thus took longer in the fluid with an expanding value of the relaxation time parameter. The temperature field decreases as a result. As seen in Fig. 8f, the thermal profile rises as the Eckert number Ec increases. When there is strong viscous dissipation in high-speed flows, heat dissipation is described by the Eckert number. In fact, since the particles are saving more energy, they become more active as Ec rises, contributing to an increase in the temperature profile.

Fig. 9 presents the effect of skin friction coefficient for emerging factors M and γ. For both M and γ, the skin friction coefficient's effect is decreasing. The effects of the magnetic and thermal stratification parameters on the fluid flow's rate of heat transfer are predicted in Fig. 10. As δ and M grow, the flow's heat transfer rate falls.

4. Conclusions

The dusty Visco-elastic Maxwell fluid's thermal stratified MHD flow across a porous stretched cylinder with the impacts of a CC heat flux model is solved using the RKF-45. Under thermal radiation, a liquid's thermal conductivity has been taken into consideration as a variable. Impacts on viscous dissipation and Joule have been investigated. The influence of the controlling factors is shown in tabular and graph form. Next, the following observations are stated:

(i) Higher ε (variable thermal conductivity) values raise the fluid's temperature.
(ii) γ's effects on the velocity profile for both phases are inversely related to those of β_1, M, K_p, and B.
(iii) Radiation and thermal stratification had opposing effects on bi-fluid temperature.
(iv) As Ec and Rd grow, so do the temperature profiles of the fluid and dust phases.
(v) The skin friction coefficient's magnitude increases as M and β_1 rise, whereas B's function decreases.
(vi) A rise in Rd and Pr values increases the local Nusselt number's magnitude.

Data availability statement

No data was used for this research and all details about our research are included in the article.

CRediT authorship contribution statement

A. Raghu: Validation, Investigation, Formal analysis. **Nagaraju Gajjela:** Writing – original draft, Supervision, Methodology, Investigation, Conceptualization. **Mahesh Garvandha:** Visualization, Software.

Declaration of competing interest

The authors declare that there is no conflict of interest our manuscript.

References

[1] F. Lin, C. Liu, P. Zhang, On hydrodynamics of viscoelastic fluids, Commun, Pure Appl. Math. 58 (2005) 1437–1471, https://doi.org/10.1002/cpa.20074.
[2] M. Jamil, C. Fetecau, C. Fetecau, Unsteady flow of viscoelastic fluid between two cylinders using fractional Maxwell model, Acta Mech. Sin. 28 (2012) 274–280, https://doi.org/10.1007/s10409-012-0043-5.
[3] T. Javed, A. Ghaffari, Numerical study of non-Newtonian maxwell fluid in the region of oblique stagnation point flow over a stretching sheet, J. Mech. 32 (2016) 175–184, https://doi.org/10.1017/jmech.2015.94.
[4] S. Afzal, H. Qi, M. Athar, M. Javaid, M. Imran, Exact solutions of fractional maxwell fluid between two cylinders, Open J. Math. Sci. 1 (2017) 52–61, https://doi.org/10.30538/oms2017.0006.
[5] N. Sadiq, M. Imran, C. Fetecau, N. Ahmed, Rotational motion of fractional Maxwell fluids in a circular duct due to a time-dependent couple, Bound, Value Probl. 2019 (2019) 20, https://doi.org/10.1186/s13661-019-1132-1.
[6] M. Khan, A. Ahmed, J. Ahmed, Boundary layer flow of Maxwell fluid due to torsional motion of cylinder: modeling and simulation, Appl. Math. Mech. 41 (2020) 667–680, https://doi.org/10.1007/s10483-020-2601-5.
[7] I.R. Umer Faryaz, Nazia Sultana, Mushtaque Hussain, Heat transfer of Maxwell fluid with Magnetohydrodynamic and porous effect in cylindrical region, J. Xi'an Shiyou Univ. Nat. Sci. Ed. 18 (2022) 762–774.
[8] M. Khan, A. Ahmed, M. Irfan, J. Ahmed, Analysis of Cattaneo–Christov theory for unsteady flow of Maxwell fluid over stretching cylinder, J. Therm. Anal. Calorim. 144 (2021) 145–154, https://doi.org/10.1007/s10973-020-09343-1.
[9] S. Islam, A. Dawar, Z. Shah, A. Tariq, Cattaneo–Christov theory for a time-dependent magnetohydrodynamic Maxwell fluid flow through a stretching cylinder, Adv. Mech. Eng. 13 (2021) 168781402110301, https://doi.org/10.1177/16878140211030152.
[10] C. Liu, M.U. Khan, M. Ramzan, Y.-M. Chu, S. Kadry, M.Y. Malik, R. Chinram, Nonlinear radiative Maxwell nanofluid flow in a Darcy–Forchheimer permeable media over a stretching cylinder with chemical reaction and bioconvection, Sci. Rep. 11 (2021) 9391, https://doi.org/10.1038/s41598-021-88947-5.
[11] M. Gayatri, K. Jayarami Reddy, M. Jayachandra Babu, Nonlinear convective flow of maxwell fluid over a slendering stretching sheet with heat source/sink, J. Appl. Comput. Mech. 8 (2022) 60–70.
[12] I.O. Abiodun A. Opanuga, Olasunmbo O. Agboola, Hilary I. Okagbue, Transient hydromagnetic maxwell fluid flow over inclined stretching surface with thermal radiation, Viscous Dissipation and Ohmic Heating Effects (2023), https://doi.org/10.21203/rs.3.rs-3379582/v1.
[13] K. Sudarmozhi, D. Iranian, I. Khan, M.A.M. Ashmaig, A.S.A. Omer, Thermofluid of Maxwellian type past a porous stretching cylinder with heat generation and chemical reaction, Int. J. Thermofluids 20 (2023) 100444, https://doi.org/10.1016/j.ijft.2023.100444.
[14] P.T. Manjunatha, B.J. Gireesha, B.C. Prasannakumara, Effect of radiation on flow and heat transfer of MHD dusty fluid over a stretching cylinder embedded in a porous medium in presence of heat source, Int. J. Appl. Comput. Math. 3 (2017) 293–310, https://doi.org/10.1007/s40819-015-0107-x.
[15] M. Radhika, R.J. Punith Gowda, R. Naveenkumar, Siddabasappa, B.C. Prasannakumara, Heat transfer in dusty fluid with suspended hybrid nanoparticles over a melting surface, Heat Transf. 50 (2021) 2150–2167, https://doi.org/10.1002/htj.21972.
[16] R.S. Varun Kumar, R.J. Punith Gowda, R. Naveen Kumar, M. Radhika, B.C. Prasannakumara, Two-phase flow of dusty fluid with suspended hybrid nanoparticles over a stretching cylinder with modified Fourier heat flux, SN Appl. Sci. 3 (2021) 384, https://doi.org/10.1007/s42452-021-04364-3.
[17] M. Garvandha, G. Nagaraju, D. Kumar, A.J. Chamkha, Study of different heating effects on two-phase flow of magnetized couple stresses over a permeable stretching cylinder with velocity slip and radiation, Int. J. Appl. Comput. Math. 8 (2022) 249, https://doi.org/10.1007/s40819-022-01444-9.
[18] N. Gajjela, M. Garvandha, D. Kumar, Heat transfer in couple stress two-fluid flow model: effects of modified heat flux, electromagnetic force, and uneven heat source/sink, Comput. Therm. Sci. An Int. J. 15 (2023) 1–14, https://doi.org/10.1615/ComputThermalScien.2023045515.
[19] B.J. Gireesha, P. Venkatesh, N.S. Shashikumar, B.C. Prasannakumara, Boundary layer flow of dusty fluid over a radiating stretching surface embedded in a thermally stratified porous medium in the presence of uniform heat source, Nonlinear Eng. 6 (2017), https://doi.org/10.1515/nleng-2016-0058.
[20] M. Bilal, M. Sagheer, S. Hussain, Numerical study of magnetohydrodynamics and thermal radiation on Williamson nanofluid flow over a stretching cylinder with variable thermal conductivity, Alexandria Eng. J. 57 (2018) 3281–3289, https://doi.org/10.1016/j.aej.2017.12.006.
[21] S. Farooq, M. Awais, M. Naseem, T. Hayat, B. Ahmad, Magnetohydrodynamic peristalsis of variable viscosity Jeffrey liquid with heat and mass transfer, Nucl. Eng. Technol. 49 (2017) 1396–1404, https://doi.org/10.1016/j.net.2017.07.013.
[22] T. Hayat, S. Farooq, B. Ahmad, A. Alsaedi, Consequences of variable thermal conductivity and activation energy on peristalsis in curved configuration, J. Mol. Liq. 263 (2018) 258–267, https://doi.org/10.1016/j.molliq.2018.04.109.
[23] S.Z. Abbas, S. Farooq, Y.M. Chu, W. Chammam, W.A. Khan, A. Riahi, H.A. Rebei, M. Zaway, Numerical study of nanofluid transport subjected to the collective approach of generalized slip condition and radiative phenomenon, Arab. J. Sci. Eng. 46 (2021) 6049–6059, https://doi.org/10.1007/s13369-020-05297-6.
[24] S. Farooq, T. Shoaib, S.Z.B. Bukhari, A.S. Alqahtani, M.Y. Malik, S. Abdullaev, S.E. Alhazmi, Peristaltic motion of Jeffrey fluid with nonlinear mixed convection, Heliyon 9 (2023) e21451, https://doi.org/10.1016/j.heliyon.2023.e21451.
[25] M. Ijaz, M. Ayub, Thermally stratified flow of Jeffrey fluid with homogeneous-heterogeneous reactions and non-Fourier heat flux model, Heliyon 5 (2019) e02303, https://doi.org/10.1016/j.heliyon.2019.e02303.
[26] G. Lakshmi Devi, H. Niranjan, S. Sivasankaran, Chemical reaction, radiation and activation energy effects on MHD buoyancy induced nanofluid flow past a vertical surface, Sci. Iran. 29 (2021) 90–100, https://doi.org/10.24200/sci.2021.56835.4934.
[27] N. Abbas, W. Shatanawi, K. Abodayeh, T.A.M. Shatnawi, Comparative analysis of unsteady flow of induced MHD radiative Sutterby fluid flow at nonlinear stretching cylinder/sheet: variable thermal conductivity, Alexandria Eng. J. 72 (2023) 451–461, https://doi.org/10.1016/j.aej.2023.04.016.
[28] A. Paul, J. Mani Nath, T. Kanti Das, An investigation of the MHD Cu-Al2O3/H2O hybrid-nanofluid in a porous medium across a vertically stretching cylinder incorporating thermal stratification impact, J. Therm. Eng. 7 (2023) 799–810, https://doi.org/10.18186/thermal.1300847.

[29] W.A. Khan, S. Farooq, S. Kadry, M. Hanif, F.J. Iftikhar, S.Z. Abbas, Variable characteristics of viscosity and thermal conductivity in peristalsis of magneto-Carreau nanoliquid with heat transfer irreversibilities, Comput. Methods Programs Biomed. 190 (2020) 105355, https://doi.org/10.1016/j.cmpb.2020.105355.

[30] S.Z. Abbas, M.K. Nayak, F. Mabood, A.S. Dogonchi, Y. Chu, W.A. Khan, Darcy Forchheimer electromagnetic stretched flow of carbon nanotubes over an inclined cylinder: entropy optimization and quartic chemical reaction, Math. Methods Appl. Sci. (2020) 1–23, https://doi.org/10.1002/mma.6956.

[31] N. Abbas, W. Shatanawi, F. Hasan, Z. Mustafa, Thermodynamic flow of radiative induced magneto modified Maxwell Sutterby fluid model at stretching sheet/cylinder, Sci. Rep. 13 (2023) 16002, https://doi.org/10.1038/s41598-023-40843-w.

[32] A.S. Butt, A. Ali, A. Mehmood, Numerical investigation of magnetic field effects on entropy generation in viscous flow over a stretching cylinder embedded in a porous medium, Energy 99 (2016) 237–249, https://doi.org/10.1016/j.energy.2016.01.067.